

## 漂浮型 BiFeO<sub>3</sub>/膨胀珍珠岩的制备及其可见光催化性能

张进\* 郭迎春 刘婵璐 徐丹  
(南京晓庄学院环境科学学院, 南京 211171)

**摘要:** 利用水热法制备了新颖的、漂浮型的膨胀珍珠岩(EP)负载 BiFeO<sub>3</sub>(BiFeO<sub>3</sub>/EP)复合光催化材料。采用 X 射线衍射(XRD)、傅里叶变换红外光谱(FT-IR)、扫描电子显微镜(SEM)、透射电子显微镜(TEM)、X 射线光电子能谱仪(XPS)和紫外可见漫反射(UV-Vis-DRS)对制备的复合材料进行了表征与分析。SEM 和 TEM 结果清楚地表明 BiFeO<sub>3</sub> 纳米粒子已被负载到 EP 表面。与纯 BiFeO<sub>3</sub> 相比, BiFeO<sub>3</sub>/EP 复合材料明显提高了对可见光的吸收能力, 减小了带隙宽度, 在可见光下对亚甲基蓝(MB)的降解表现出更强的光催化活性。其中, 70%BiFeO<sub>3</sub>/EP 复合材料对 MB 染料废水的光催化活性最高, 其光催化反应一级速率常数是纯 BiFeO<sub>3</sub> 的 2.2 倍。由于质轻中空的特点, 制备的 BiFeO<sub>3</sub>/EP 颗粒漂浮在液面上, 有利于相分离和反应后光催化剂的回收。材料的重复性试验表明, 复合材料在 MB 光降解过程中是相当稳定的。

**关键词:** BiFeO<sub>3</sub>; 膨胀珍珠岩; 光催化; 可见光

中图分类号: O643.32 文献标识码: A 文章编号: 1001-4861(2021)05-0905-09

DOI: 10.11862/CJIC.2021.091

## Synthesis and Visible-Light-Driven Photocatalytic Properties of Floating BiFeO<sub>3</sub>/Expanding Perlite Photocatalysts

ZHANG Jin\* GUO Ying-Chun LIU Chan-Lu XU Dan  
(School of Environmental Science, Nanjing Xiaozhuang University, Nanjing 211171, China)

**Abstract:** A series of floating photocatalysts containing BiFeO<sub>3</sub> nanoparticles on the expanding perlite (EP) support were synthesized by hydrothermal method. The as-prepared composites were characterized by X-ray diffraction (XRD), Fourier transform infrared spectrometer (FT-IR), scanning electron microscope (SEM), transmission electron microscopy (TEM), X-ray photoelectron spectra (XPS) and UV-Vis diffusion reflection (UV-Vis DRS). The SEM and TEM analyses indicated that BiFeO<sub>3</sub> was dispersed on the surface of EP. The DRS spectra revealed that the composites had improved optical adsorption in the visible light region, and exhibited enhanced photocatalytic activity for methylene blue (MB) degradation under visible light irradiation. It was found that the 70%BiFeO<sub>3</sub>/EP composite showed the highest photocatalytic activity for MB dye wastewater treatment, and the first-order rate constant for 70%BiFeO<sub>3</sub>/EP was 2.2 times higher than that for pure BiFeO<sub>3</sub>. Owing to the low density of EP, the as-prepared BiFeO<sub>3</sub>/EP particles floated in water to favor phase separation and the recovery of the photocatalyst after the reaction. The recovery test shows that the composite was rather stable during the MB photodegradation.

**Keywords:** BiFeO<sub>3</sub>; expanded perlite; photocatalysis; visible light

With the development of economy and the rapid increase of population, a large number of industrial sewage has been produced, which has caused serious harm to China's water resources and environment. The

收稿日期: 2020-09-28。收修改稿日期: 2021-01-10。

中国博士后基金(No.2012M511254)和江苏省大学生创新训练计划项目(No.201711460054x)资助。

\*通信联系人。E-mail: jzmary@163.com

pollution of water resources is also gradually deteriorating, which has a great impact on our lives. Dye waste water, which mainly comes from the production of dyes and dye intermediates, has the characteristics of high content of organic matter, high toxicity and difficult treatment. Therefore, it is urgent to adopt effective methods to treat dye waste water. Photocatalysis is an advanced oxidation technique which utilizes the clean solar energy and environment friendly semiconductors<sup>[1]</sup>. Many studies have shown that photocatalysis can effectively degrade dye waste water<sup>[2-3]</sup>.

In past decades, titania ( $\text{TiO}_2$ ) semiconductor has been the utmost utilized photocatalyst. However,  $\text{TiO}_2$  can be only excited under UV light irradiation, which accounts for 4% of the total solar energy. This limits the practical application of  $\text{TiO}_2$  as a photocatalyst<sup>[4-5]</sup>. Currently, preparation of visible-light-driven catalysts has attracted much attention. Among them,  $\text{BiFeO}_3$  as a ferroelectric material has become a hot one in the field of photocatalysis due to its narrow band gap and photovoltaic effect.  $\text{BiFeO}_3$  exhibits excellent visible light photocatalytic activity for the degradation of organic dyes and removal of organic compounds<sup>[6-8]</sup>. However, there are some limitations of  $\text{BiFeO}_3$  when it is used as catalyst. It is always in the form of powder, easy to agglomerate. It usually suspends into the solution which leads to reduce the using rate of light. The solid-liquid separation and catalyst recovery after the reaction is also a problem. To prepare supported  $\text{BiFeO}_3$  catalysts can solve the restrictions. Therefore, various supports have been used to immobilize the nano and/or micro catalysts, like activated carbon<sup>[9]</sup>, natural materials<sup>[10]</sup>, fly ash cenospheres<sup>[11]</sup>. In this work, we choose expanded perlite (EP) as the support material.

EP is a kind of acid glassy rock. After being extracted at high temperature, crushed and screened, EP has a porous structure, can float on the water surface due to low density, and has good adsorption performance for organic matters<sup>[12-14]</sup>. The main constituents of EP are silica, alumina and other metal oxides. EP is abundant in China and is a cheap and eco-friendly material commonly used in industry and construction.

Based on the lightweight and porous properties of EP, combined with the efficient photocatalytic performance of  $\text{BiFeO}_3$ , novel  $\text{BiFeO}_3/\text{EP}$  composites were prepared in this work. Their enhanced photocatalytic activity was evaluated by the degradation of methylene blue (MB) under visible light irradiation.

## 1 Experimental

### 1.1 Materials

EP was obtained from Yushun Insulation Material Factory located in Shandong Province of China. All other chemicals used in the experiment are analytical pure, obtained from Sinopharm Group Chemical Reagent Co., Ltd. De-ionized water was used in all experiments.

### 1.2 Material preparation

First, EP particles were sieved uniformly through a 200-mesh screen mesh, then were soaked in 5%  $\text{HNO}_3$  solution for 1 h, dried in oven at 80 °C, and then they were calcined in muffle furnace at 500 °C for 2 h, then cooled at room temperature, and the white powders were obtained.

A hydrothermal method was used to synthesize the  $\text{BiFeO}_3/\text{EP}$  photocatalysts. Firstly, 1 mmol  $\text{Bi}(\text{NO}_3)_3 \cdot 5\text{H}_2\text{O}$  and 1 mmol  $\text{Fe}(\text{NO}_3)_3 \cdot 9\text{H}_2\text{O}$  were separately dissolved in 15 mL deionized water under continuous stirring. The Bi precursor solution was added gradually to the Fe precursor solution (solution A). Then, 5 mol·L<sup>-1</sup> potassium hydroxide solution was added dropwise into solution A, and we mixed them under magnetic stirrer for about 30 min to obtain a brownish yellow mixture (solution B). Next, a certain amount of EP powder was immersed in 30 mL of deionized water and the resulted mixture was stirred for 30 min at room temperature (solution C). Solution B was added gradually to solution C and the resulted solution was stirred for 30 min at room temperature. Then the resulting suspension was hydrothermally treated in a Teflon-lined stainless steel autoclave at 160 °C for 24 h. After the autoclave was naturally cooled to room temperature, the product was filtrated and washed several times with deionized water and ethanol. Finally, the product was dried in an

oven at 80 °C for 8 h. According to the above methods, BiFeO<sub>3</sub>/EP composite photocatalysts with 25%, 50%, 70% and 80% can be prepared, respectively. The percentages (25%, 50%, 70% and 80%) represent the mass fraction of BiFeO<sub>3</sub> deposited particles.

### 1.3 Materials characterization

XRD pattern was filed by using a Bruck D8 advance X-ray diffractometer with Cu K $\alpha$  ( $\lambda=0.154$  nm). The tube current was 40 mA and the tube voltage was 40 kV, and the scanning range ( $2\theta$ ) was 10°~80°, with a scanning rate of 0.02 (°)·s<sup>-1</sup>. The molecular structure of the sample was determined by Nicolet 5700 infrared spectrometer (FT - IR). The morphological studies of as-synthesized samples were determined on transmission electron microscope, high resolution transmission electron microscope (TEM and HRTEM, FEI Tecnai G2 F20) and scanning electron microscope (SEM, sigma 500 of Carl Zeiss company). Diffuse reflectance spectroscopy (DRS) was performed on an Avantes (Ava Lamp-DH-S Ava spec 2048-Tec) and BaSO<sub>4</sub> was used as the blank reference. Photoluminance (PL) spectra of the samples were measured using a Perkin Elmer LS 55 fluorescence spectrophotometer. Nitrogen adsorption-desorption curve was recorded by Micrometrics (ASAP 2020). X-ray photoelectron spectroscopy (XPS, Perkin Elmer PHI 5000) was applied to investigate the surface elemental composition. The source generated Al K $\alpha$  radiation, the test voltage was 12 kV, and the power was 700 W.

### 1.4 Photocatalytic experiment

The photocatalytic efficiencies of as-synthesized samples were measured by photocatalytic degradation of MB (10 mg·L<sup>-1</sup>) utilizing a 300 W Xe lamp operating cut-off-filter ( $\lambda > 420$  nm). Before photocatalytic process, the aqueous suspension including 1 g·L<sup>-1</sup> of photocatalysts was maintained in the dark under stirring for 30 min to reach adsorption-desorption equilibrium. Then, it was exposed to the visible-light source. After a given irradiation time, 4 mL of dispersion was removed and separated from the photocatalyst. MB was analyzed by UV-visible spectrum at their characteristic peak (664 nm) to determine content remaining.

## 2 Results and discussion

### 2.1 XRD patterns

The XRD patterns of EP, BiFeO<sub>3</sub>, BiFeO<sub>3</sub>/EP are shown in Fig. 1. In Fig. 1a, the characteristic peaks at  $2\theta$  of 22.6°, 32.2°, 39.7°, 45.6°, 51.3°, 56.5°, 57.1°, 66.4° and 67.2° correspond to (012), (110), (202), (024), (122), (018), (214), (208) and (220) planes of BiFeO<sub>3</sub> (PDF No.71-2494). The diffraction peak of EP (Fig. 1f) did not show the obvious and sharp diffraction peaks, indicating that EP is a kind of amorphous material. As shown in Fig. 1b~1e, both the peaks of BiFeO<sub>3</sub> and EP were observed in the XRD patterns of the composites. Owing to the relatively low diffraction intensity of EP, an arc shape was observed in the XRD patterns of the composites<sup>[15-16]</sup>.

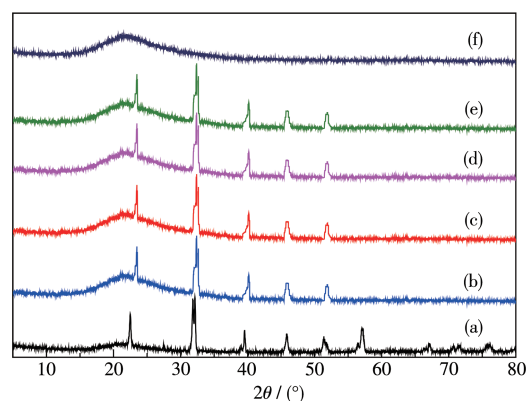


Fig.1 XRD patterns of (a) BiFeO<sub>3</sub>, (b) 25%BiFeO<sub>3</sub>/EP, (c) 50%BiFeO<sub>3</sub>/EP, (d) 70%BiFeO<sub>3</sub>/EP, (e) 80%BiFeO<sub>3</sub>/EP and (f) EP

### 2.2 FT-IR spectra analysis

Fig. 2 displays the FT-IR spectra of EP, pure BiFeO<sub>3</sub> and BiFeO<sub>3</sub>/EP. As shown in Fig. 2a, the strong band around 560 cm<sup>-1</sup> is assigned to the stretching vibration of Fe—O in BiFeO<sub>3</sub>. The band at 520 cm<sup>-1</sup> corresponds to the bending vibration of O—Fe—O in BiFeO<sub>3</sub><sup>[17]</sup>, and the peak at 642 cm<sup>-1</sup> belongs to the vibration of Bi—O in the BiO<sub>6</sub> octahedra<sup>[18-19]</sup>. The band at 1 681 cm<sup>-1</sup> is due to the hydroxyl O—H bending vibration. For EP (Fig. 2f), the band at 1 572 cm<sup>-1</sup> is due to the C=C bending vibration, while the absorption bands at 1 045 and 721 cm<sup>-1</sup> are assigned to the Si—O (Si—O—Si and Si—O—Al) stretching vibrations<sup>[20-21]</sup>. Fig. 2b~2e show the spectra of BiFeO<sub>3</sub>/EP

composites with different mass fractions of  $\text{BiFeO}_3$ . The characteristic bands of  $\text{BiFeO}_3$  and EP were observed. However, in the spectra of  $\text{BiFeO}_3/\text{EP}$  composites, most of EP characteristic bands appeared with lower intensity, which is possibly ascribed to the coordination and electrostatic attraction between  $\text{BiFeO}_3$  and EP in  $\text{BiFeO}_3/\text{EP}$  composites<sup>[16,22]</sup>. Moreover, as shown in Fig.2b~2e, the band at  $3\,435\text{ cm}^{-1}$  has higher intensity

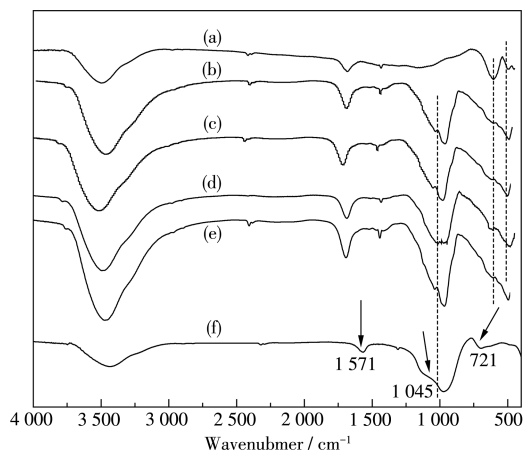


Fig.2 FT-IR spectra of (a)  $\text{BiFeO}_3$ , (b) 70% $\text{BiFeO}_3/\text{EP}$ , (c) 50% $\text{BiFeO}_3/\text{EP}$ , (d) 25% $\text{BiFeO}_3/\text{EP}$ , (e) 80% $\text{BiFeO}_3/\text{EP}$  and (f) EP

than that of EP, and the band at  $3\,342\text{ cm}^{-1}$  is assigned to the  $\text{—OH}$  stretching mode of adsorbed water molecules, which play an important role in the photocatalytic activity because these groups can inhibit the recombination of photogenerated charges<sup>[23-24]</sup>.

### 2.3 SEM and EDX analysis

Fig.3a describes the SEM micrographs of EP. The powder of EP had lamellar disordered structure. Moreover, the surface of EP particles had some irregularly shaped-open pores, which can keep it floating on the water surface for a long time and contribute to the absorption of organic matters molecules. Fig. 3b describes SEM micrographs of  $\text{BiFeO}_3$ . The products were irregular particles, and the small particles were basically agglomerated in one up. Fig.3c reveals the surface of EP after immobilization of  $\text{BiFeO}_3$  particles on them, and the agglomeration of particles was lessened. The TEM image (Fig. 3d) also shows that the  $\text{BiFeO}_3$  particles are successfully deposited on the surface of EP. As shown in Fig.4, EDS analysis of the  $\text{BiFeO}_3/\text{EP}$  confirmed the presence of Bi, Fe, Si, Al, K and O elements.

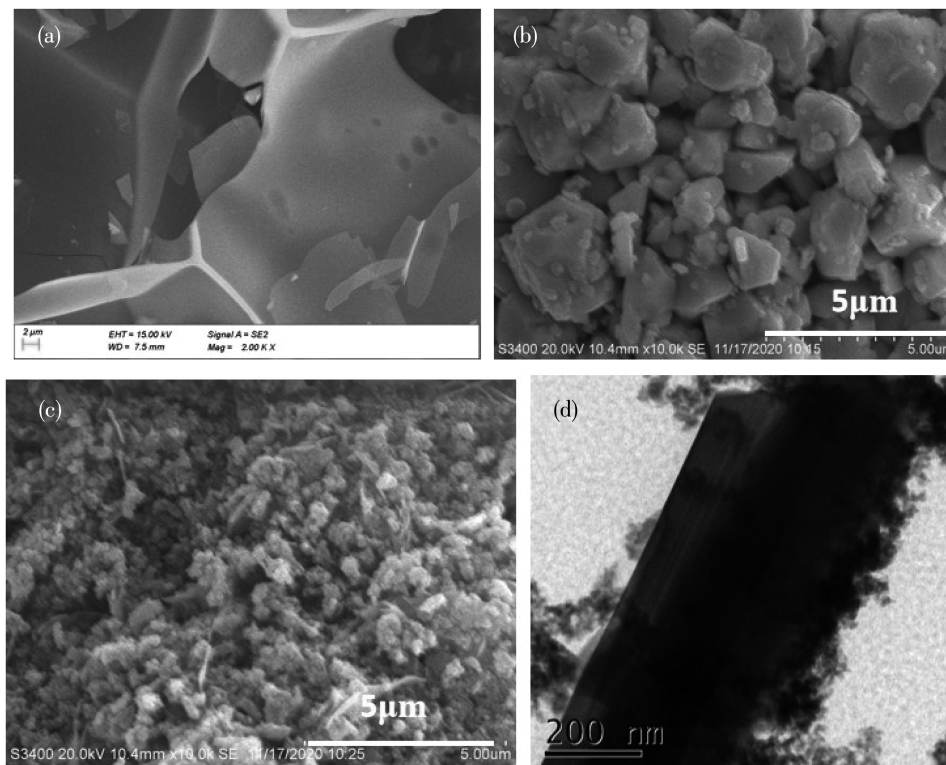
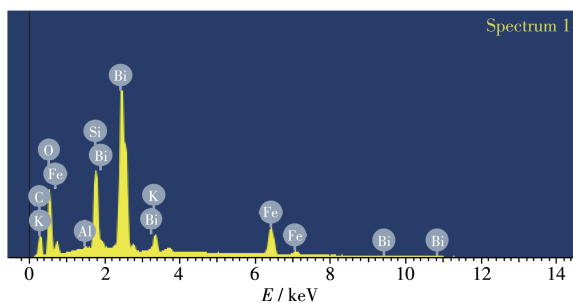


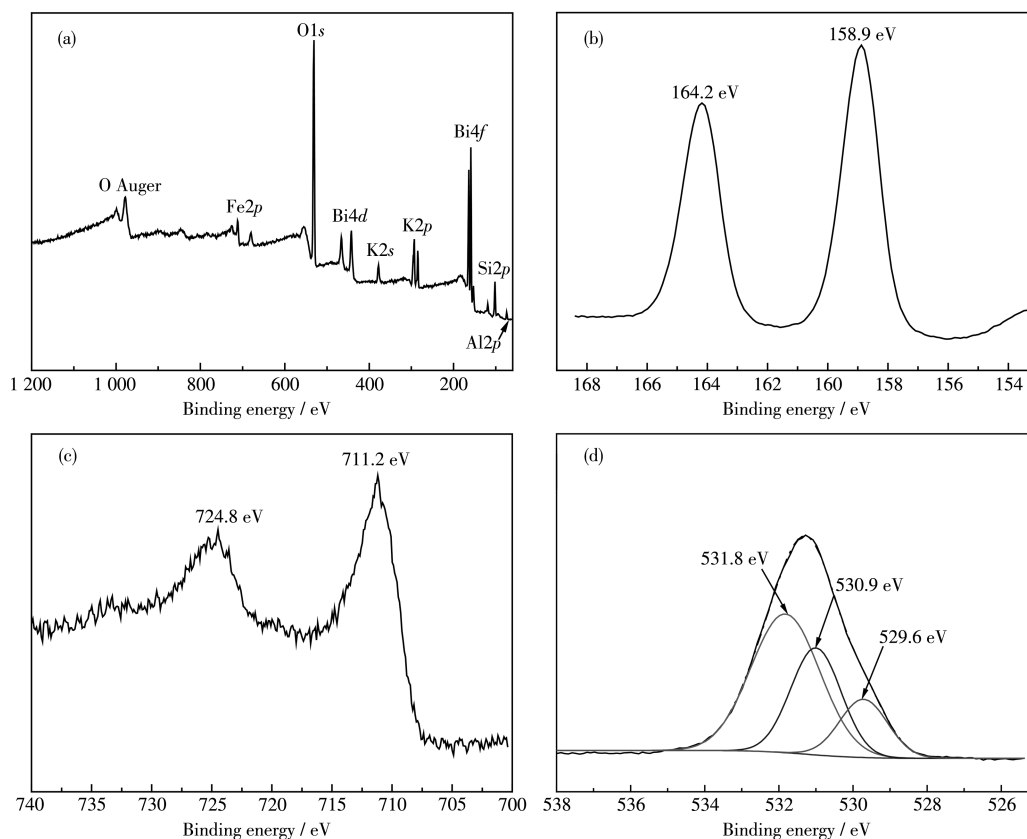
Fig.3 SEM images of (a) EP, (b)  $\text{BiFeO}_3$ , (c) 70% $\text{BiFeO}_3/\text{EP}$  and TEM image of (d) 70% $\text{BiFeO}_3/\text{EP}$

Fig.4 EDS of 70%BiFeO<sub>3</sub>/EP

## 2.4 XPS analysis

In order to investigate the nature of the surface species involved into the catalysts, high-resolution XPS spectra were collected from 70%BiFeO<sub>3</sub>/EP composite. Fig.5a shows the full spectrum of this composite. It can be seen that the material mainly contains elements

such as Fe, Bi, K, O, Si and Al. The Bi4*f* spectrum (Fig.5b) showed two distinct peaks at 158.9 and 164.2 eV, which correspond to Bi4*f*<sub>7/2</sub> and Bi4*f*<sub>5/2</sub>, respectively. And it shows that Bi element exists in the form of Bi<sup>3+</sup> oxide. Fig.5c is the XPS spectrum of 2*p* orbital of Fe. The two characteristic peaks correspond to Fe2*p*<sub>3/2</sub> and Fe2*p*<sub>1/2</sub>, and the binding energies were 711.2 and 724.8 eV, respectively. It shows that Fe exists in the form of Fe<sup>3+</sup>. Fig.5d exhibits spectra of oxygen (O1*s*), and the O1*s* peaks at 529.6 and 530.9 eV are corresponding to Fe—O and Bi—O, respectively<sup>[25-26]</sup>. The O1*s* peak of 531.8 eV corresponds to the chemisorption of oxygen, which is attributed to O<sub>2</sub><sup>2-</sup> in EP (Al<sub>2</sub>O<sub>3</sub> and SiO<sub>2</sub>)<sup>[27]</sup>.

Fig.5 XPS spectra of 70%BiFeO<sub>3</sub>/EP: (a) full survey spectra, (b) Bi4*f*, (c) Fe2*p* and (d) O1*s*

## 2.5 BET and BJH analysis

The N<sub>2</sub> adsorption-desorption isotherms and BJH (Barrette-Joyner-Halenda) pore-size distributions of EP and 70%BiFeO<sub>3</sub>/EP are displayed in Fig. 6. The N<sub>2</sub> adsorption - desorption isotherm of the samples were

close to the type IV of hysteresis loops, confirming the mesoporous structure of the samples according to the IUPAC classification<sup>[16]</sup>. The BET (Brunauer-Emmett-Teller) specific surface area, pore size and total pore volume of the samples are shown in Table 1. Compar-

ing the BET surface area of the samples reveals that deposition of BiFeO<sub>3</sub> on EP can increase its surface area from 4 to 72 m<sup>2</sup>·g<sup>-1</sup> and the pore volume also increased from 0.006 9 to 0.40 cm<sup>3</sup>·g<sup>-1</sup>. The average pore diameter of the EP and 70%BiFeO<sub>3</sub>/EP were 6.5 and 23.7 nm, respectively. The mesopores were formed

by the agglomeration and connection of adjacent particles in the sample. This network nanostructure offers more efficient transportation for reactant molecules to the active sites, resulting enhanced photocatalytic activity<sup>[16,23,28]</sup>.

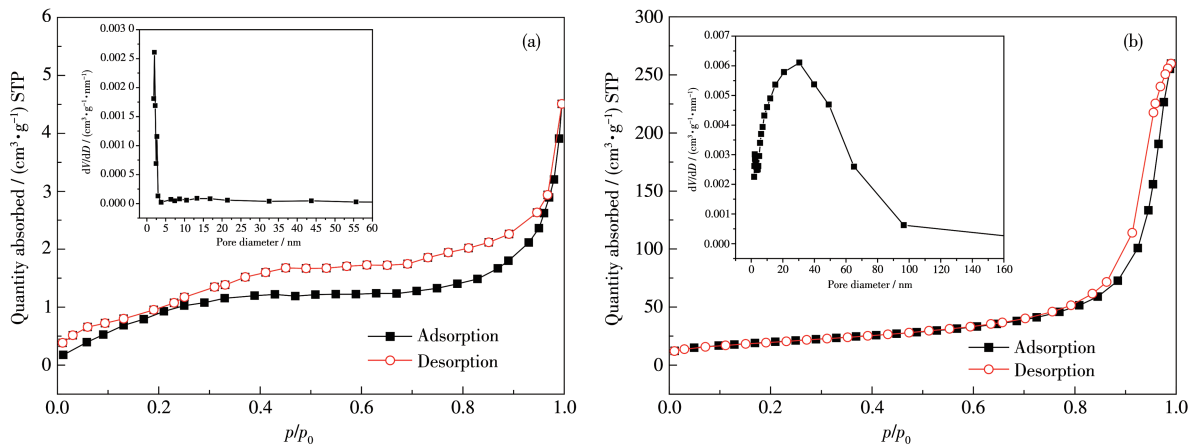


Fig.6 N<sub>2</sub> adsorption-desorption isotherms and corresponding pore size distribution curves (inset) of as-synthesized samples: (a) EP and (b) 70%BiFeO<sub>3</sub>/EP

**Table 1** Specific surface area, pore size and total pore volume distribution of EP and 70%BiFeO<sub>3</sub>/EP

Sample	Specific surface area / (m <sup>2</sup> ·g <sup>-1</sup> )	Pore size / nm	Total pore volume / (cm <sup>3</sup> ·g <sup>-1</sup> )
EP	4	6.5	0.006 9
70%BiFeO <sub>3</sub> /EP	72	23.6	0.40

## 2.6 DRS analysis

Fig. 7a depicts the UV - Vis DRS of EP, BiFeO<sub>3</sub> and 70%BiFeO<sub>3</sub>/EP. As displayed in Fig. 7a, the pure EP had only one certain absorption in the ultraviolet region of  $\lambda < 400$  nm and no absorption in the visible region, indicating that the carrier has no photocatalytic activity under visible light. However, the BiFeO<sub>3</sub> and 70%BiFeO<sub>3</sub>/EP samples had broad absorption in both ultraviolet region and visible region. Compared with the pure BiFeO<sub>3</sub>, 70%BiFeO<sub>3</sub>/EP exhibited strong absorption in the visible-light region. And the absorption edges were shifted toward the longer wavelength side (red shift).

The band gap energy ( $E_g$ ) could be calculated, by plotting  $(\alpha h\nu)^2$  vs  $h\nu$  using Eq. 1:  $\alpha h\nu = A(h\nu - E_g)^n$ , where  $\alpha$ ,  $h$ ,  $\nu$ , and  $A$  are the absorption coefficient, Planck constant, the frequency of light, and a constant, respectively<sup>[29]</sup>. As shown in Fig. 7b, direct band gap energy for pure BiFeO<sub>3</sub> and BiFeO<sub>3</sub>/EP was 2.21 and 2.09 eV,

respectively. The results show that the band gap was reduced and the response to visible light was improved after incorporation of EP with BiFeO<sub>3</sub>.

Photoluminescence (PL) emission spectrum was performed to analyze the separation, transfer and capture of photocarriers on the surface of the sample. Generally speaking, the lower photoluminescence intensity is, the lower recombination rate of the electron-hole pairs over the photocatalyst is<sup>[15-16]</sup>. Fig. 7c shows the PL spectra with 300 nm excitation wavelength for different samples. Pure BiFeO<sub>3</sub> exhibited a broad peak at 465 nm, whereas this kind of emission peak gradually diminished in BiFeO<sub>3</sub>, 25%BiFeO<sub>3</sub>/EP, 50%BiFeO<sub>3</sub>/EP and 70%BiFeO<sub>3</sub>/EP, respectively. It has been reported that EP can provide an efficient electron transport track to the metal semiconductor material loaded on its surface, and inhibit the recombination of photogenerated electron-hole pairs<sup>[15,22]</sup>. In Fig. 7c, 70%BiFeO<sub>3</sub>/EP possessed the lowest PL intensity, implying better photoin-

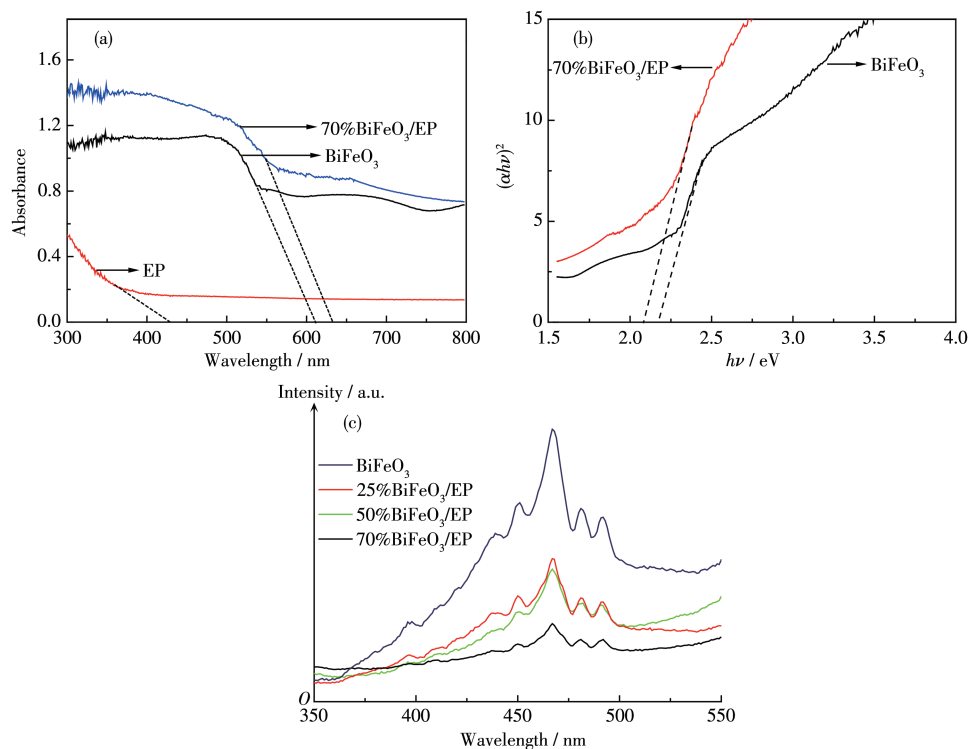


Fig.7 (a) UV-Vis DRS spectra, (b) band gaps (EP excluded) and (c) PL spectra of as-prepared samples

duced  $e^-/h^+$  separation efficiency and enhanced photocatalytic activity. The band gap shifted to the longer wavelength side (red shift) and decrease of PL intensity could lead to an improved photocatalytic activity<sup>[23-24,27]</sup>.

## 2.6 Photocatalytic performance

The photocatalytic activity of the as-prepared photocatalysts was investigated by degrading water-soluble organic contaminants MB under visible light irradiation. Fig. 8a shows the adsorption and photocatalytic degradation curves of as-prepared samples. After a continuing stirring for 30 min in darkness to reach the adsorption-desorption equilibrium, the pure EP particles absorbed MB molecules and the absorption percentage for MB was 25% of the dark reaction. When the light turned on, the absorption percentage of MB hardly changed, indicating that pure EP had no photocatalytic effect on MB. However, the BiFeO<sub>3</sub>/EP catalyst showed better photocatalytic degradation efficiency than that of pure BiFeO<sub>3</sub>. With the increase of the loading concentration, the activity increased. The highest photocatalytic activity was obtained by 70%BiFeO<sub>3</sub>/EP composite, with a MB decoloration of 94% within 180 min. When the mass fraction of BiFeO<sub>3</sub> was up to 80%,

the activity of BiFeO<sub>3</sub>/EP composite decreased. The excess BiFeO<sub>3</sub> species was confined on the surface of EP, which might block the pores on the EP surface, reducing the adsorption capacity of the EP to MB molecules<sup>[30-31]</sup>. Fig.8b depicts the first-order kinetic simulation of MB photodegradation catalyzed by as-prepared samples. And the apparent rate constants ( $k$ , min<sup>-1</sup>) were determined from the Eq.2:  $\ln(c_t/c_0) = -kt$ , where  $c_t$  is the diesel concentration (mg·L<sup>-1</sup>) of MB at time  $t$  (min);  $c_0$  is the concentration of MB at the beginning of photocatalytic reaction. The  $k$  values of BiFeO<sub>3</sub>, 25%BiFeO<sub>3</sub>/EP, 50%BiFeO<sub>3</sub>/EP, 70%BiFeO<sub>3</sub>/EP, 80%BiFeO<sub>3</sub>/EP were 0.005 47, 0.007 15, 0.009 02, 0.012 1, 0.010 7 min<sup>-1</sup>, respectively. The result clearly demonstrated that 70%BiFeO<sub>3</sub>/EP has the largest  $k$  value, indicating that the material has the best photocatalytic performance.

In addition, the stability of photocatalytic materials has an important impact on its practical application. In order to study the reusability of the as-prepared samples, four photocatalytic cycles were carried out with 70%BiFeO<sub>3</sub>/EP as an example. After each cycle, the catalyst was filtered, washed and dried, and then

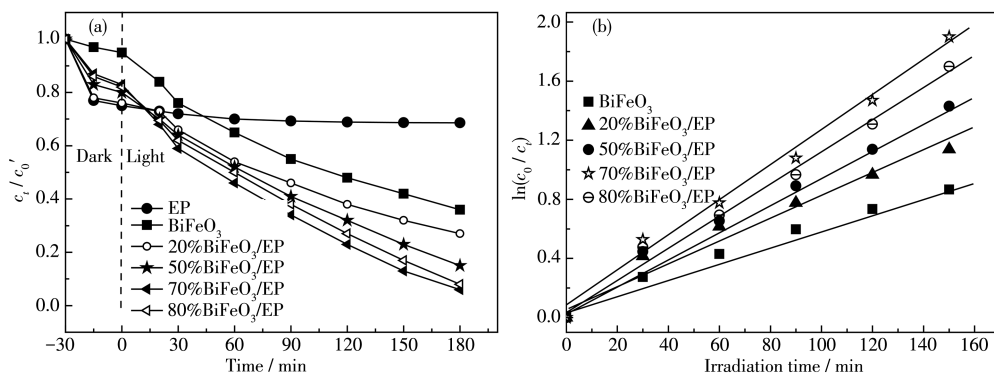


Fig.8 (a) Adsorption and photocatalytic performance ( $c_0'$  is the initial concentration of MB) and (b) first-order kinetic fitting lines of MB degradation by as-prepared samples under visible light

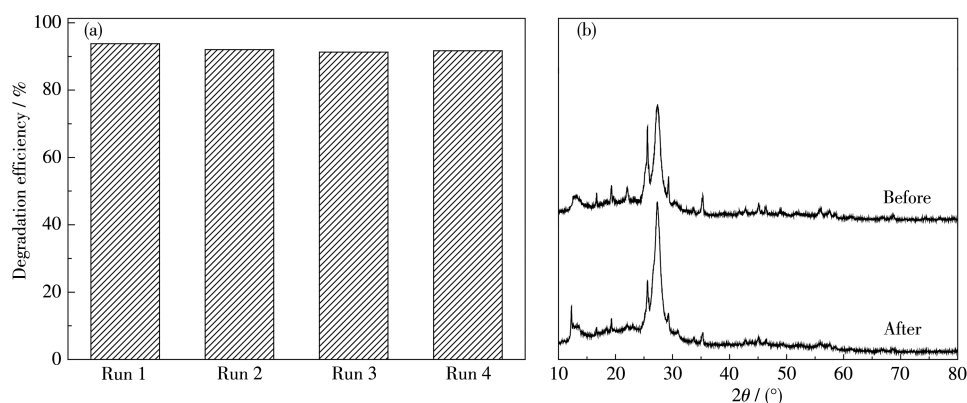


Fig.9 (a) Degradation efficiency of MB over 70%BiFeO<sub>3</sub>/EP in different recycling runs and (b) XRD patterns of 70%BiFeO<sub>3</sub>/EP before and after the photocatalytic degradation of MB

added to the fresh MB solution to continue the experiment. As shown in Fig.9a, it clearly indicates that no obvious loss occurred in the photocatalytic efficiency after 4 consecutive runs.

From the analysis of XRD patterns of 70%BiFeO<sub>3</sub>/EP composite before and after the cycle experiment (Fig.9b), it was almost same to as-fabricated fresh sample, and the composite after cycle experiment still maintained the characteristic peak of BiFeO<sub>3</sub>. These results verify the unique advantage of applying EP as a sustainable support in recycling and stabilizing of 70%BiFeO<sub>3</sub>/EP composite<sup>[32]</sup>.

### 3 Conclusions

The floating BiFeO<sub>3</sub>/EP composites were successfully synthesized by hydrothermal method. The performance of BiFeO<sub>3</sub>/EP with different mass fractions of BiFeO<sub>3</sub> were investigated. TEM images showed that needle-like BiFeO<sub>3</sub> particles was densely distributed

on the surface of EP. The DRS spectra showed that the band gap was reduced and the response to visible light was improved after incorporation of EP with BiFeO<sub>3</sub>. The highest photocatalytic activity was obtained by 70%BiFeO<sub>3</sub>/EP composite, with a MB decoloration of 94% within 3 h, and the first-order rate constant for 70%BiFeO<sub>3</sub>/EP was 2.2 times higher than that for pure BiFeO<sub>3</sub>. After four consecutive runs, no obvious loss occurred in the photocatalytic efficiency of 70%BiFeO<sub>3</sub>/EP. Owing to the low density of EP, the as-prepared BiFeO<sub>3</sub>/EP composites can float in water. This favors phase separation by filtration to recover these photocatalysts after reaction. In addition, EP have the advantages of low cost. Therefore, the composite catalyst is promising for practical applications in water purification due to excellent recyclability, high efficiency, and good stability. In particular, these floating BiFeO<sub>3</sub>/EP photocatalysts are expected to be used in the treatment of surface oil pollution and oil spills.

## References:

- [1] Sandoval A, Hernández-Ventura C, Klimova T E. *Fuel*, **2017**,**198**:22-30
- [2] Mills A, Davies R H, Worsley D. *Chem. Soc. Rev.*, **1993**,**22**:417-425
- [3] Waiskopf N, Ben-Shahar Y, Banin U. *Adv. Mater.*, **2018**,**30**:1-10
- [4] Akira F, Kenichi H. *Nature*, **1972**,**238**:37-38
- [5] AlSalka Y, Granone L I, Ramadan W, Hakki A, Bahnemann D W. *Appl. Catal. B*, **2019**,**244**:1065-1095
- [6] Gao F, Chen X Y, Yin K B, Dong S A, Ren Z F, Yuan F, Yu T, Zou Z G, Liu J M. *Adv. Mater.*, **2007**,**19**:2889-2892
- [7] Han F M, Ye X, Chen Q, Long H M, Rao Y F. *Sep. Purif. Technol.*, **2020**,**232**:115967-115977
- [8] Wang N, Luo X D, Han L, Zhang Z Q, Zhang R Y, Olin H, Yang Y. *Nano-Micro Lett.*, **2020**,**81**(12):1-23
- [9] Jiao S, Zhao Y M, Li C S, Wang B S, Qu Y. *Green Energy Environ.*, **2019**,**4**:66-74
- [10] 宋萃, 赵丽华, 戚明颖, 孙榕尉, 祝茜. 无机化学学报, **2020**,**36**(3):521-528  
SONG C, ZHAO L H, QI M Y, SUN R W, ZHU Q. *Chinese J. Inorg. Chem.*, **2020**,**36**(3):521-528
- [11] Zhang J, Li Q, Cui H, Zhai J P. *J. Environ. Sci.*, **2014**,**26**(9):1936-1942
- [12] Chen F X, Zhang Y H, Liu J G, Wang X K, Chu P K, Chu B H, Zhang N. *Constr. Build. Mater.*, **2020**,**249**:118728-118730
- [13] Khan U A, Liu J J, Pan J B, Ma H C, Zuo S L, Yu Y C, Ahmad A, Iqbal M, Ullah S, Li B S. *Ind. Eng. Chem. Res.*, **2019**,**58**:9286-9299
- [14] Kapeluszna E, Kotwica L, Pichór W, Nocuń-Wczelik W. *Sustainable Mater. Technol.*, **2020**,**24**:231-242
- [15] Qiu H X, Hu J W, Zhang R, Gong W T, Yu Y C, Gao H W. *Colloids Surf. A*, **2019**,**583**:123996-124004
- [16] Darkhosha F, Lashanizadegana M, Mahjoubb A R, Khavar A H. *Solid State Sci.*, **2019**,**91**:61-72
- [17] Salimi Z, Hosseini S A. *Fuel*, **2019**,**239**:1204-1212
- [18] Murshed M M, Nénert G, Burianek M, Robben L, Mühlberg M, Schneider H, Fischer R X, Gesing T M. *J. Solid State Chem.*, **2013**, **197**:370-378
- [19] Hu Z T, Liu J C, Yan X L, Oh W D, Lim T T. *Chem. Eng. J.*, **2015**, **262**:1022-1032
- [20] Jiang L, Wang J, Wu X, Zhang G. *Water Air Soil Pollut.*, **2017**,**228**:463-474
- [21] Majouli A, Younsi S A, Tahiri S, Albizane A, Loukili H, Belhaj M. *Desalination*, **2011**,**277**:61-66
- [22] Khan U A, Liu J J, Pan J B, Ma H C, Zuo S L, Yu Y C, Ahmad A, Li B S. *Mater. Sci. Semicond. Process.*, **2018**,**83**:201-210
- [23] Wang X, Wang W, Wang X J, Zhang J, Gu Z L, Zhou L J, Zhao J F. *RSC Adv.*, **2015**,**5**:41385-41392
- [24] Liu G, Han C, Pelaez M, Zhu D, Liao S, Likodimos V, Kontos A G, Falaras P, Dionysiou D D. *J. Mol. Catal. A: Chem.*, **2013**,**372**:58-65
- [25] Dixit T K, Sharma S, Sinha A S. *Inorg. Chem. Commun.*, **2020**,**117**:107945-107953
- [26] Patel S K, Lee J H, Kim M K. *J. Mater. Chem. C*, **2018**,**6**:526-534
- [27] Khan U A, Liu J J, Pan J B, Zuo S L, Ma H C, Yu Y C, Ahmad A, Ullah S, Li B S. *Dalton Trans.*, **2018**,**47**:12253-12263
- [28] Antonelli D M, Ying Y. *Angew. Chem. Int. Ed.*, **1995**,**34**:2014-2017
- [29] Wang D S, Wang Y H, Li X Y, Luo Q Z, An J, Yue H X. *Catal. Commun.*, **2008**,**9**:1162-1166
- [30] Asiltürk M, Sener S. *Chem. Eng. J.*, **2012**,**180**:354-363
- [31] Zhang J, Cui H, Wang B, Li Q, Zhai J P. *Appl. Surf. Sci.*, **2014**,**300**:51-57
- [32] Xu H Y, Jia W H, Ren S L, Wang J Q. *Chem. Eng. J.*, **2018**,**337**:10-18